Experimental investigation on FRP-reinforced surface cracked steel plates subjected to cyclic tension

Li, Zongchen; Jiang, Xiaoli; Hopman, Hans; Zhu, Ling; Liu, Zhiping; Tang, Weiguo

DOI
10.1080/15376494.2020.1746448

Publication date
2020

Document Version
Final published version

Published in
Mechanics of Advanced Materials and Structures

Citation (APA)
Li, Z., Jiang, X., Hopman, H., Zhu, L., Liu, Z., & Tang, W. (2020). Experimental investigation on FRP-reinforced surface cracked steel plates subjected to cyclic tension. *Mechanics of Advanced Materials and Structures*, *28 (2021)*(24), 2551-2565. https://doi.org/10.1080/15376494.2020.1746448

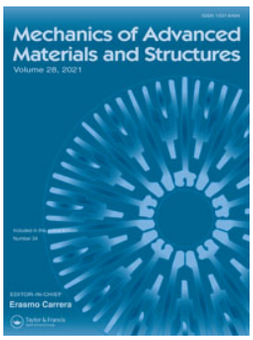

Mechanics of Advanced Materials and Structures

ISSN: (Print) (Online) Journal homepage: https://www.tandfonline.com/loi/umcm20

Experimental investigation on FRP-reinforced surface cracked steel plates subjected to cyclic tension

Zongchen Li, Xiaoli Jiang, Hans Hopman, Ling Zhu, Zhiping Liu & Weiguo Tang

To cite this article: Zongchen Li, Xiaoli Jiang, Hans Hopman, Ling Zhu, Zhiping Liu & Weiguo Tang (2021) Experimental investigation on FRP-reinforced surface cracked steel plates subjected to cyclic tension, Mechanics of Advanced Materials and Structures, 28:24, 2551-2565, DOI: 10.1080/15376494.2020.1746448

To link to this article: https://doi.org/10.1080/15376494.2020.1746448

Published online: 14 Apr 2020.

MECHANICS OF ADVANCED MATERIALS AND STRUCTURES
2021, VOL. 28, NO. 24, 2551–2565
https://doi.org/10.1080/15376494.2020.1746448

Taylor & Francis
Taylor & Francis Group

ORIGINAL ARTICLE

Experimental investigation on FRP-reinforced surface cracked steel plates subjected to cyclic tension

Zongchen Li[a], Xiaoli Jiang[a], Hans Hopman[a], Ling Zhu[b], Zhiping Liu[c], and Weiguo Tang[b]

[a]Department of Maritime and Transport Technology, Delft University of Technology, Delft, The Netherlands; [b]Department of Naval Architecture, Ocean and Structural Engineering, School of Transportation, Wuhan University of Technology, Wuhan, PR China; [c]Port Logistic Technology and Equipment Research Centre of Ministry of Education, Wuhan, PR China.

ABSTRACT

Surface cracked steel plates reinforced with single-side Fiber-Reinforced Polymer (FRP) subjected to cyclic tension are experimental studied. The main purpose is to analyze the effect of FRP reinforcement on the crack growth. The failure modes and their effects are analyzed as well. Given the single-side reinforcement, reinforcing the cracked surface significantly prolonged the fatigue life, while reinforcing the reversed side resulted in the opposite consequence. Most specimens did not encounter debonding failures, indicating such failures are avoidable by improving the reinforcement quality. The results also indicate the bond layer number is an insensitive factor – an optimum number is existed.

ARTICLE HISTORY
Received 14 February 2020
Accepted 19 March 2020

KEYWORDS
Debonding; fatigue crack growth rate; fatigue test; FRP reinforcement; surface crack

Nomenclature

a	crack depth of surface cracks
a_0	notch depth
a/c	aspect ratio of surface cracks
a/t	normalized crack depth
b	plate width
C	Paris' law constant
c	half crack length of surface cracks
c_0	notch length
da/dN	crack growth rate along the depth direction
dc/dN	crack growth rate along the length direction
E_i	elastic modulus
E_s, E_c, E_g, E_a	elastic modulus of the steel plate, CFRP, GFRP, and adhesive layer along the length direction
F	remote tensile force on the steel plate
H	bending correction factor for the Newman-Raju's equation
G_{ij}	shear modulus
K_I, K_{Ia}, K_{Ic}	Stress Intensity Factor (SIF), the SIF of the deepest point and the surface point of the surface crack
M	out-of-plane bending moment
N	cyclic index
Nu	Poisson's ratio
Q	Boundary correction factor of the surface crack
R	load ratio
T	tensile strength
t	thickness of the FRP-reinforced steel plates
Δt	the distance between the centroid of the steel plate and the centroid of the FRP reinforced steel plate
t_s, t_c, t_g, t_a	thickness of the steel plate, CFRP, GFRP, and adhesive layer respectively
σ_0	in-plane tensile stress in the steel plate without FRP reinforcement
σ_t, σ_b	in-plane tensile stress and bending stress in the steel plate with FRP reinforcement

1. Introduction

Surface cracks frequently initiate from the surface of metallic structures due to surface damages, fretting corrosion, or corrosion pitting [1–3]. They might continually propagate under cyclic loads, causing serious threats to the structural integrity. In practical situations, preventing surface cracks from propagating to through-thickness cracks is of great importance, such as in the fields of aerospace engineering [4], transportation pipelines [5, 6], pressure vessels, and nuclear reactors [7, 8].

Fiber-Reinforced Polymer (FRP) reinforcement is a recognized alternative of traditional fatigue crack repairing methods, such as bolting, welding, and drilling a stop hole [9–13]. It has been highly valued for the outstanding advantages in terms of effectiveness, time-saving, cost-effective, no secondary damage, and ease of installation [14–16]. The efficiency of FRP reinforcement has been certificated that it can significantly decrease the fatigue crack growth rate (FCGR) and prolong the residual fatigue life of the cracked metallic structures. In past a few decades, the FRP reinforcement on through-thickness cracks in metallic structures has been applied and investigated. The majority of the investigations were conducted in steel plates. Among these studies, cracks initiated from either wedge-shape notches at the edge of a metallic structure or from a drilling hole located in the middle of the specimen. Three main loading conditions which are tension, bending or their combined loads were discussed [17–19]. By means of these studies, the mechanism of the FRP reinforcement on through-thickness cracks was

CONTACT Zongchen Li z.li-8@tudelft.nl Department of Maritime and Transport Technology, Delft University of Technology, 2628 CD Delft, The Netherlands.

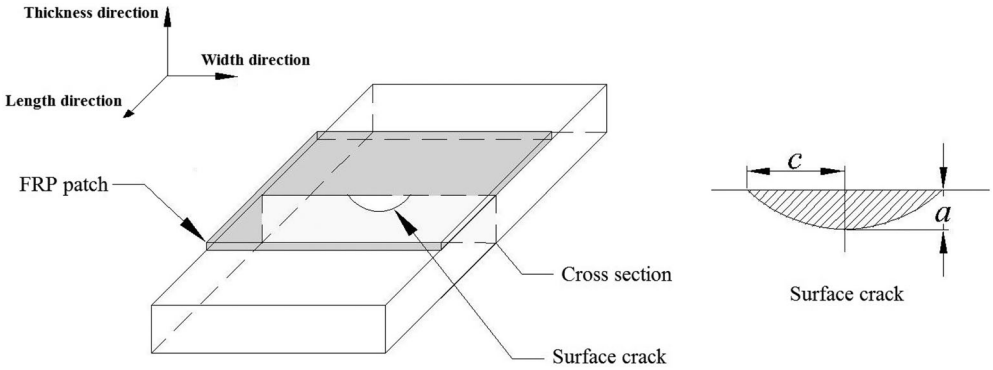

Figure 1. The sketch diagram of the single-side FRP-reinforced surface cracked specimen.

Table 1. Material properties of GFRP.

E_1 (Pa)	E_2 (Pa)	T (Pa)	G_{13} (Pa)	G_{23} (Pa)	Nu
72×10^9	72×10^9	1.1×10^9	4.7×10^9	3.5×10^9	0.33

Table 2. Material properties of the CFRP material.

E_1 (Pa)	E_2 (Pa)	T (Pa)	G_{13} (Pa)	G_{23} (Pa)	Nu
230×10^9	25×10^9	4.9×10^9	5.5×10^9	3.9×10^9	0.3

Table 3. Material properties of the resin epoxy.

E (Pa)	T (Pa)	G (Pa)	Nu
2.8×10^9	70×10^6	1.4×10^9	0.35

gradually understood [20], the failure modes during the fatigue process were discussed as well, such as interface failures between adhesive and steel/FRP, cohesive failure, FRP delamination, and FRP rupture [14].

To date, the investigation of FRP reinforcement on surface cracked metallic structures is seriously insufficient. Yet it cannot directly refer to the studies on reinforcing the through-thickness cracks, because: the possible failure modes of using FRP to reinforce surface cracks in metallic structure is unclear, thus its effects on surface crack growth is undefined; surface crack grows as a semi-elliptical shape, the effect of FRP reinforcement on three-dimensional surface crack growth is unclear. For example, in recent years, researcher indicated that the crack-induced debonding is very likely to occur which may generate negative influence on the FRP reinforcement toward the FCGR decrease [21–24]. While the effectiveness of such failure on FRP reinforced surface cracked metallic structures has not been studied. In addition to that, the available studies mainly concentrated on the metallic structures in the civil engineering domain; while surface cracked metallic structures such as in aerospace engineering, offshore piping industry usually bear higher load amplitude, which might affect the failure modes during the fatigue process [21]. Although the FRP reinforcement on internal surface cracked pipes has been studied recently [24, 25], the possible failure modes and their influence on surface crack growth have not been identified since the surface cracks which located in the internal surface of the pipes did not contact with the FRP laminates. Further and in-depth studies are in a great demand in order to facilitate the application and development of FRP reinforcement on surface cracked metallic structures.

Given that, we conduct an experimental investigation on surface cracked steel plates reinforced with the single-side FRP patch. The main purpose of this study is to analyze the effectiveness of FRP reinforcement on surface crack growth, the possible failure modes and their effects on the surface crack growth are discussed as well. The cyclic tensile load, as a primary load case, is adopted in order to better understand the mechanism of FRP reinforcement on surface cracks in metallic structures. In Section 2, the specimen preparation processes are introduced. In Section 3, the test set-up is described. The failure modes and test results are presented in Section 4 and discussed in Section 5, respectively. Finally, the conclusions are drawn in Section 6.

2. Specimen preparation

Specimen preparation is an important step for the sake of achieving ideal experimental results. The preparation of the FRP-reinforced surface cracked steel plate specimens required a certain number of steps: the selection of four different materials, i.e., steel substrate, adhesive, Glass-FRP (GFRP), and Carbon-FRP (CFRP); notch manufacturing; pre-cracking and FRP reinforcement. The quality of each constituent part is needed to be guaranteed. In this section, the preparation procedures are step-by-step introduced.

2.1. Material properties

The sketch diagram of the single-side FRP-reinforced surface cracked specimen is shown in Figure 1. The specimens contained four materials: the steel substrate, GFRP, CFRP, and adhesive. Stainless steel of 907A for subsea scenarios conforming to GJB 6055-2007 code [26] has been used as the steel substrate. The steel material has yield strength of 390 MPa, and tensile strength of 530 MPa. In light of the galvanic corrosion between CFRP laminates and steel substrate, one layer of GFRP laminate was adopted as the first layer of the FRP patch. The GFRP laminate applied the E-glass fiber weave fabric while the CFRP laminate used the T700S series unidirectional fabric. Their material properties are listed in Tables 1 and 2, respectively. The adhesive adopted the resin epoxy conforming to the code GB/T 2567-2008 [27] and its material properties are listed in Table 3. Note the material properties of the steel, FRP and adhesive are all provided by each manufacturer.

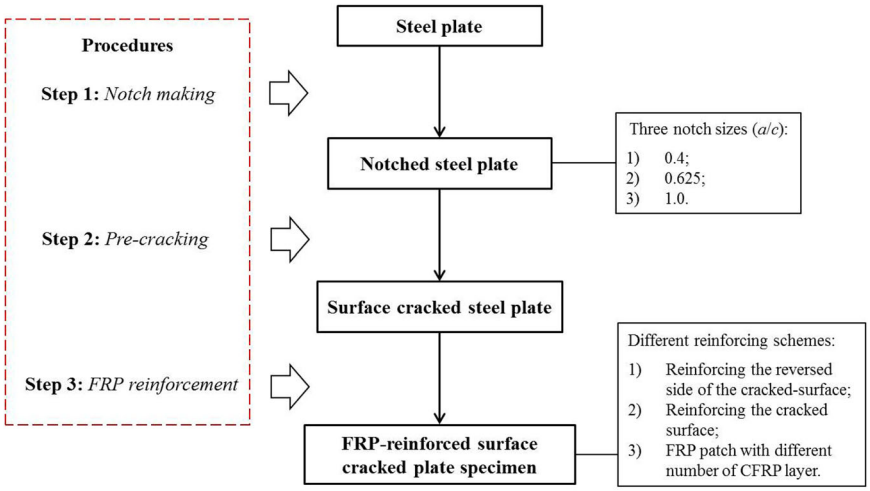

Figure 2. The procedure of specimen preparation.

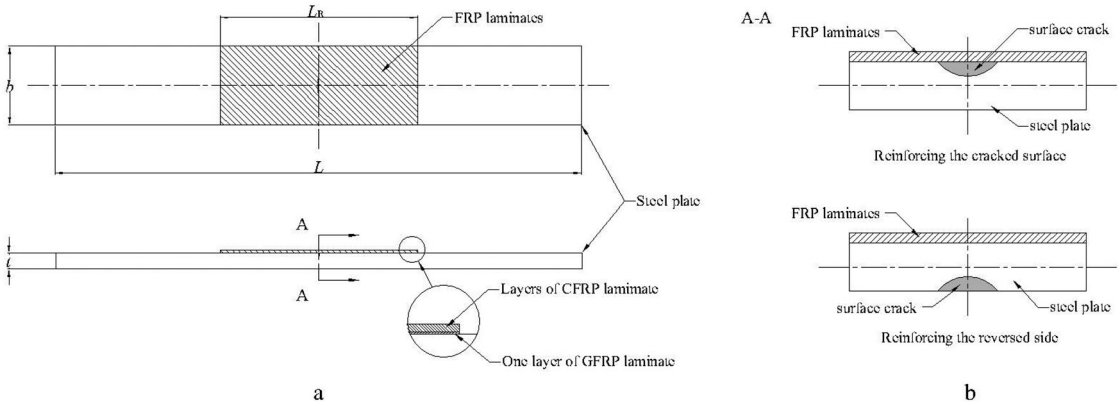

Figure 3. The configuration of specimens: a) a FRP reinforced steel plate; b) the location of a surface crack in a steel plate.

2.2. Specimen manufacturing

The manufacturing of the specimens contains three main steps: notch manufacturing, pre-cracking, and the FRP reinforcement, as shown in Figure 2. In order to guarantee that the surface cracks are semi-elliptical shaped, semi-elliptical notches were manufactured, located in the middle of the steel plates, orienting perpendicular to the length direction of the steel plate, as indicated in Figure 3. The notches were made by Micro-Electric Discharging Machining (Micro-EDM) suggested by ASME E2899 in order to achieve the user designed notch profile and to avoid the thermal residual stress [28]. The aimed aspect ratio of the notches is 0.4, 0.625, and 1.0, representing some common seen surface cracks in metallic structures in practical situations [29, 30]. The width of the notch is controlled as 0.35 mm. The details of the notch size are listed in Table 4.

It should be noted that the notches were not yet fatigue cracks, thus before using the FRP patch to reinforce the steel plates, a pre-cracking procedure was conducted to generate fatigue surface cracks initiated from the notches [31]. The pre-cracking procedure was conducted on the fatigue machine containing two stages: the first stage adopted 80% yield stress as the load amplitude of the constant amplitude sinusoidal cyclic loading, while the second stage adopted 60% yield stress respectively. Note that both of the two stages were under the load ratio equals to $R = 0.1$. During each stage, tensile fatigue load was applied on the specimens until the surface crack initiated from the notch and propagated more than 1.0 mm. Then the size of each surface crack after the pre-cracking procedure was regarded as the initial crack size. The specimens, therefore, were ready for the FRP reinforcement procedure.

Afterwards, the specimens were reinforced with the FRP patch on either the cracked surface or its reversed side by hand lay-up technique. The FRP patch was bonded in the middle of the specimen. The reinforcement procedure contained the surface preparation, cleaning, composite laminates pasting. Finally, the FRP laminates were compressed by a large mass in order to squeeze redundant resin epoxy and eliminate the bubbles in the interlaminations, as well as to let the each laminate bonded tightly. Then the specimens were placed at room temperature for solidification of one week, in order to achieve the optimum bond condition.

2.3. Specimens configurations

The steel plate is 400 mm long and 60 mm wide, with an approximately 12.30 mm thickness. The width of each GFRP and CFRP laminate equals to the width of steel specimen, while the length of the FRP patch is 150 mm. The thickness

Table 4. Specimens' configuration and reinforcement details.

Group	Specimen	Notch category	b (mm)	t (mm)	a_0 (mm)	c_0 (mm)	The reinforced surface	No. of CFRP layer
1	S-1(1)	1	59.86	12.39	1.90	5.00	/	/
	S-1(2)	1	59.95	12.33	1.86	5.00	/	/
	S-1(3)	1	59.86	12.36	1.92	4.98	/	/
2	S-2(1)	2	59.87	12.32	1.96	3.15	/	/
	S-2(2)	2	59.43	12.36	1.90	3.15	/	/
	S-2(3)	2	59.87	12.36	1.96	3.14	/	/
3	S-3(1)	3	59.80	12.39	3.98	4.00	/	/
	S-3(2)	3	59.78	12.43	3.96	3.98	/	/
	S-3(3)	3	59.69	12.45	3.95	3.98	/	/
4	SI-1-R(1)	1	59.45	12.30	1.96	5.00	The reversed side	4
	SI-1-R(2)	1	59.92	12.28	1.86	4.95	The reversed side	4
	SI-1-R(3)	1	59.85	12.34	1.86	4.95	The reversed side	4
5	SE-1-R(1)	1	59.79	12.41	1.90	5.02	The cracked surface	4
	SE-1-R(2)	1	59.67	12.34	1.90	4.86	The cracked surface	4
	SE-1-R(3)	1	60.02	12.36	1.88	4.99	The cracked surface	4
6	SE-2-R(1)	2	60.01	12.41	1.91	3.10	The cracked surface	4
	SE-2-R(2)	2	59.52	12.42	1.86	3.13	The cracked surface	4
	SE-2-R(3)	2	59.96	12.43	1.90	3.08	The cracked surface	4
7	SE-3-R(1)	3	59.95	12.47	3.90	3.89	The cracked surface	4
	SE-3-R(2)	3	60.13	12.38	3.90	3.94	The cracked surface	4
	SE-3-R(3)	3	59.84	12.22	3.89	3.94	The cracked surface	4
8	SE-1-R2(1)	1	60.07	12.30	1.95	4.95	The cracked surface	2
9	SE-1-R6(1)	1	60.04	12.40	1.91	5.00	The cracked surface	6

The parameters, i.e., b, t, a_0, c_0 are measured based on each specimens, each of which is the weighted average of three measurement locations.

of each layer of GFRP and CFRP laminate is 0.35 mm. Each FRP reinforced specimen applies one layer of GFRP as the first layer, and several layers of CFRP laminate on top of that, as shown in Figure 3. The configuration of the specimens and reinforcement details are shown in Table 4. In total, nine groups of 23 specimens were prepared. Group 1, 2, and 3 are three controlling group of three different groups of initial surface crack sizes without FRP reinforcement. Group 4 is using FRP to reinforce the reversed side of the cracked surface, while Group 5, 6, and 7 are using FRP to reinforce the cracked surface with different crack sizes. Most groups have three repetitive specimens except Group 8 & 9 which have only one specimen each. The name of the specimens in Table 4 represents the notch configuration, FRP reinforcement scheme, and its repetitive number. Take 'SE-1-R(1)' as an example, 'S' means steel plate, 'E' represents reinforcing the steel plate on the cracked surface, 'R' means reinforcement, the first '1' stands for the first type of notch, and the second '1' means the No. of the repetitive specimen.

3. Test set-up

The fatigue tests were carried out under constant amplitude sinusoidal cyclic loading, generated by MTS Hydraulic Actuator, which has a capacity of 250 kN. The schematic of test setup and the real test setup is shown in Figure 4. Two edges of each tensile specimen were clamped by a pair of hydraulic clamps, positioned horizontally on the fatigue machine. The load was applied in tension condition to ensure a pure tension statue for the plate specimen. Note that the fatigue test follows the code of ASTM E647 [31].

During the fatigue test, the strain on the external CFRP laminate along the crack propagation path was monitored, as shown in Figure 5(a). Four strain gauges were installed along the middle line, as indicated in Figure 5(b). The size of each strain gauge is 4.0 mm × 4.0 mm, and the distance between each adjacent strain gauge is 3.0 mm. Therefore, the gauge matrix can cover 25.0 mm × 4.0 mm of the right middle area on the external CFRP laminate. Then the gauges were connected to the dynamic strain indicator TMR^{TM}−300, which was set to record the strain data for 60 s of every 10,000 cycles until the end of the fatigue test. These data would help us to trace the crack-induced debonding during the fatigue test [21]. Note that the strain monitoring was not conducted for the specimens in Group 7.

All the fatigue tests were conducted at room temperature and air environment under load control condition. The loading frequency was set as 12.0 Hz. The load ratio R maintained 0.1 for the crack growth process of all tests. The crack growth process was recorded by Beach Marking technique by means of changing the load ratio R to 0.5 and cycle for 5,000 cycles, as described in Figure 6. Each test ended automatically once the tensile specimen fractured and trigger the displacement limiter of the fatigue machine.

4. Test results

Possible failures might occur when using CFRP to reinforce structures subjected to tension, including interfacial failures, cohesive failures, FRP delamination, and FRP ruptures [14]. In this section, the failure modes during and after each fatigue test, and the surface crack growth behavior & results of each specimen were presented.

4.1. Failure modes during the fatigue test

The failure modes of all FRP reinforced specimens during each fatigue tests are listed in Table 5. During the fatigue test, failures including cohesive failures, FRP delamination, and FRP ruptures did not occur on all specimens. After the fatigue test, along with the fracture of the steel plate, the

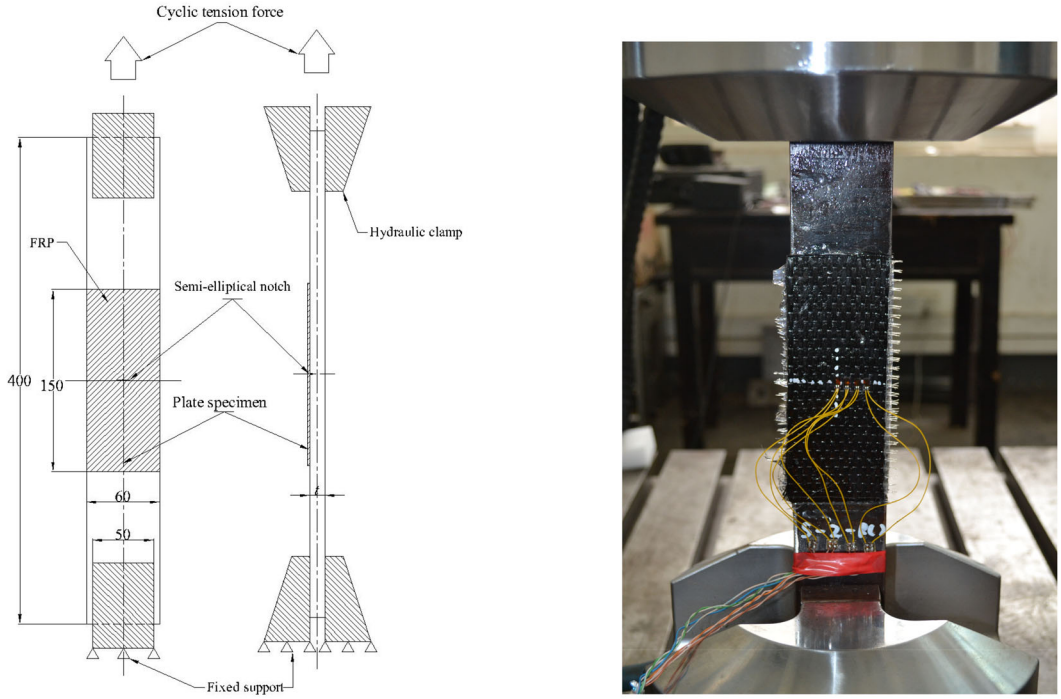

Figure 4. Specimen installation: a) the schematic; b) the actual specimen installation.

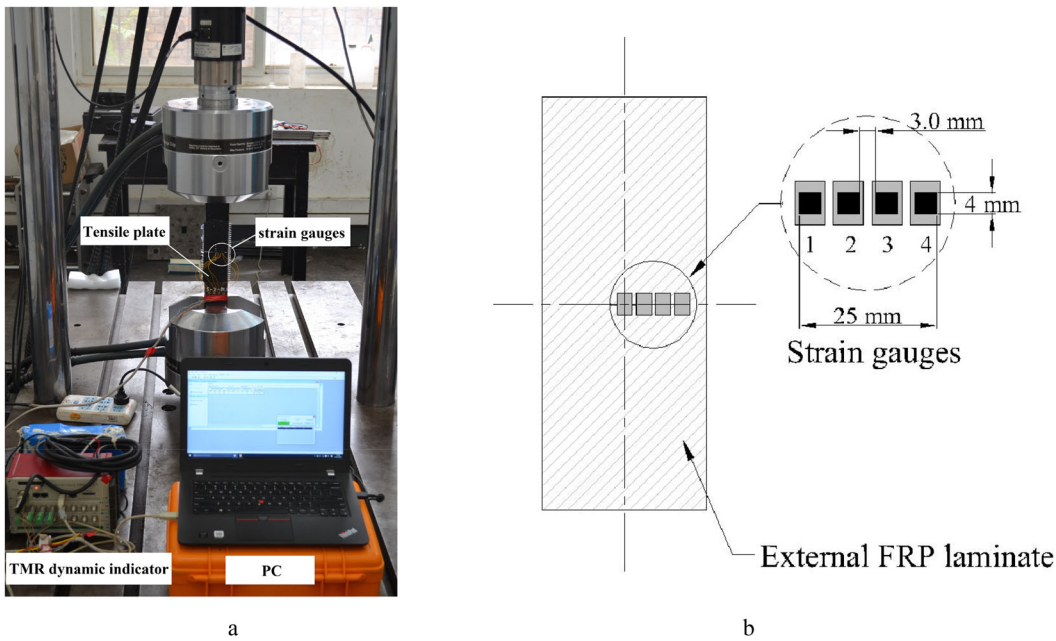

Figure 5. a) Actual fatigue test set-up; b) strain gauges distributed on the external FRP laminate.

FRP patch entirely debonded from the steel substrate of each specimen. Besides, during the fatigue test, edge debonding failures between the FRP patch and the steel substrate were observed. In total, four out of 14 specimens have encountered the edge debonding failure. These debonding failures happened either at the beginning (e.g., SE-1-R(1)) or later during the fatigue test (e.g. SE-1-R(2)), as shown in Figure 7.

When crack-induced debonding occurred, the strain on the external layer of FRP laminates around the surface cracked area would drop dramatically, owing to the fact that there is no shear stress transfer within the debonded region [21]. Therefore, the crack-induced debonding is possible to be detected using the installed strain gauge matrix. Then strain values for each specimen of every 10,000 cycles are linked to their corresponding crack length, calibrate by the cycle-index. In this study, the strain around the cracked area on the external CFRP layer was recorded, as shown in Figure 5(b).

The study of Ref. [21] indicated that when using FRP to reinforce through-thickness cracked steel plates, the crack-induced debonding would occur along with the crack

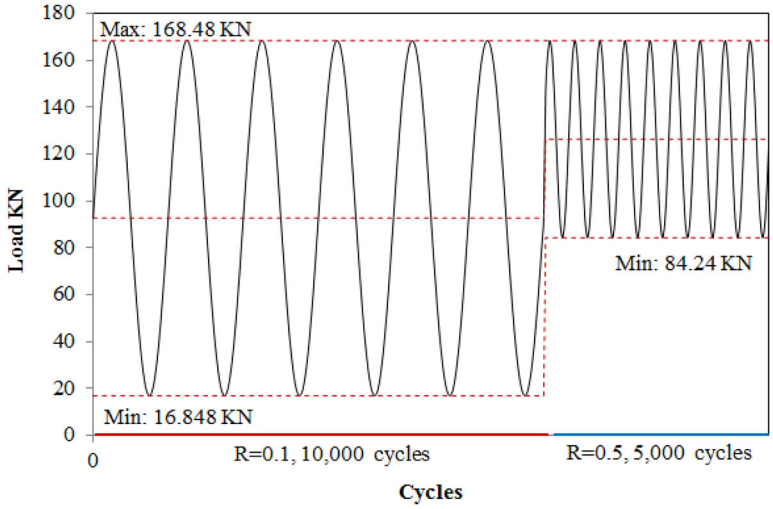

Figure 6. The load spectrum and beach mark generating procedure.

Table 5. Failure modes during the fatigue tests.

Specimen	Edge debonding	*N* when optical failure occurs	Crack-induced debonding	*c* when crack-induced debonding occurs
SI-1-R(1)	No	/	No	/
SI-1-R(2)	No	/	No	/
SI-1-R(3)	No	/	No	/
SE-1-R(1)	**Yes**	Between 30,000 ~ 40,000	**Yes**	Between 9.4 and 11.39 mm
SE-1-R(2)	**Yes**	Between 60,000 ~ 70,000	**Yes**	Between 8.8 and 10.07 mm
SE-1-R(3)	No	/	No	/
SE-2-R(1)	No	/	No	/
SE-2-R(2)	No	/	No	/
SE-2-R(3)	**Yes**	Between 70,000 ~ 80,000	**Yes**	Between 8.78 and 10.52 mm
SE-3-R(1)	No	/	No	/
SE-3-R(2)	No	/	No	/
SE-3-R(3)	No	/	No	/
SE-1-R2(1)	No	/	No	/
SE-1-R6(1)	**Yes**	Between 20,000 ~ 30,000	**Yes**	Between 9.22 and 11.27 mm

Figure 7. Edge debonding occurred during the fatigue test.

growth. While the crack-induced debonding did not occur on the majority of the specimens in this study, based on the stable strain data variation on the external CFRP laminate around the cracked area during the fatigue test. The crack-induced debonding did occur on four FRP reinforced specimens (listed in Table 5), indicated by the sudden drop of the strain value. The crack size recorded in Table 5 when the crack-induced debonding occurred indicated that the failure usually at the later stage of the fatigue tests. Besides, it often accompanied by the edge debonding.

Figure 8 shows an example of the strain data of one cycle recorded before, during and after the crack-induced debonding occurs of specimens SE-1-R(2). The name of the curve means the strain data of the corresponding strain gauge (e.g., G1 to G4 represent the four gauges, the 'Be', 'Du', and 'Af' means before, during, and after the crack-induced

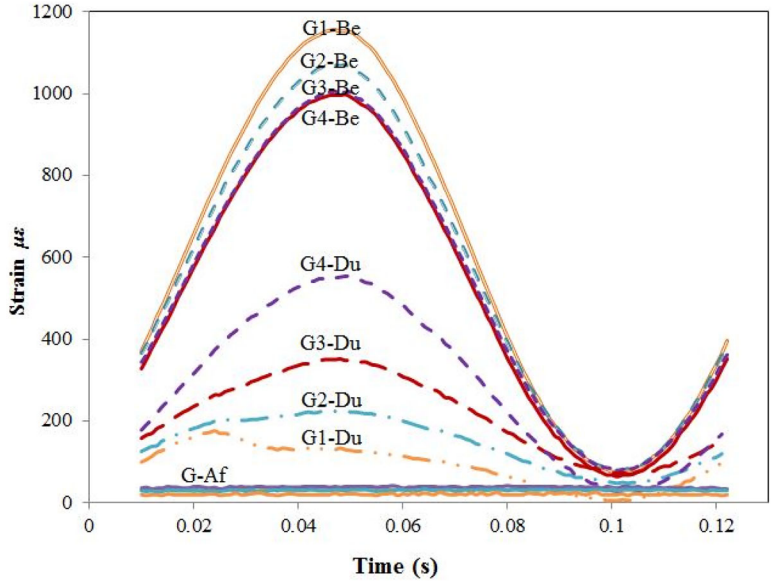

Figure 8. Strain monitoring data of before, during, and after crack-induced debonding occurs of specimen SE-1-R(2).

debonding occurred respectively). It can be seen that when the crack-induced debonding occurred, the strain monitored by the four strain gauges decreases dramatically. The monitored strain value of G1 is the smallest and the strain increases successively from G1 to G4. After the crack-induced debonding occurred, the FRP patch around the middle of the steel plate completely lost the bond to the steel substrate, resulting in the almost zero micro strain value.

4.2. Failure modes after the fatigue test

Necking phenomenon appeared at the end of the fatigue test after the surface crack penetrated the wall, as shown in Figure 9(a). Then the crack growth entered the rapid growth stage because of the limited effective sectional area, indicated by the rough cross-section surface, as shown in Figure 9(b). Eventually after the fatigue test, the FRP patch debonded from the steel substrate uniformly, as shown in Figure 9(c). No cohesive failure or FRP delamination, or FRP rupture were observed for all specimens.

4.3. Surface crack growth behavior and crack growth results

The crack growth behavior was recorded by the Beach Marking technique using an electronic reading microscope, as shown in Figure 10. One random specimen was selected from each repetitive three specimens to show the crack shape variation during the fatigue test. The cycle index between each two adjacent beach marks is 10,000. The figures clearly demonstrate the multiple initiations along the notch fronts, and the surface cracks continually propagated as a semi-elliptical shape until the crack penetrated the pipe wall. The results of crack depth and length, corresponding to the cycle-index are listed in the Table A1 in the Appendix.

5. Discussion on the crack growth results

In this section, the crack growth results of all specimens were discussed and analyzed. Because of the individual difference between each repetitive specimen in each group, after the pre-cracking procedure, the notches have propagated to different sizes. This made it impossible to directly compare the crack growth between different specimens with the same notch sizes. To facilitate the analyzing of surface crack growth, the results of crack growth along the depth/length direction versus cycle-index are modified by the interpolation method to follow the same starting crack depth. The results, therefore, are shown by the curves of crack growth along the depth/length direction versus the cycle index. In addition, since debonding failure may have a negative influence on the FCGR, the response of FCGR of each specimen was analyzed.

5.1. Using FRP to reinforce the reversed side of the cracked surface of the steel plates

In certain situations, directly reinforcing the cracked surface in a metallic structure is not feasible. In such case, reinforcing the reversed side of the cracked surface might be an alternative. In this section, the results of using FRP patch to reinforce the reversed side of the cracked surface of the steel plates are analyzed. The results of a-N & c-N and da/dN-a & dc/dN-c of the reinforced specimens are compared with the un-reinforced specimens.

The results of surface crack growth of using FRP to reinforce the reversed side of the cracked surface are shown in Figure 11(a,b). The results of S-1 and SI-1-R are consistent with each repetitive specimen, respectively. However, rather than prolonging the residual fatigue life, the FRP reinforcement slightly shortened the fatigue life. The reason is that besides the positive effects in terms of decreasing the stress distribution, the FRP reinforcement have generated an out-of-plane bending moment on the steel plate owing to

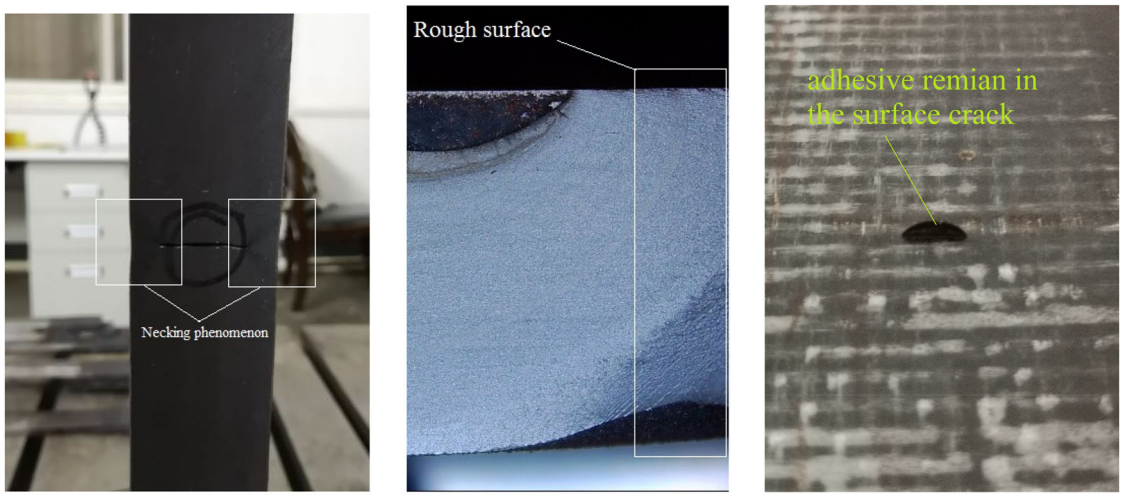

Figure 9. Failure modes after the fatigue tests: a) necking phenomenon appeared at the end of the fatigue test; b) rough fracture surface of the specimens after the fatigue test; c) uniform debonding after the fatigue test.

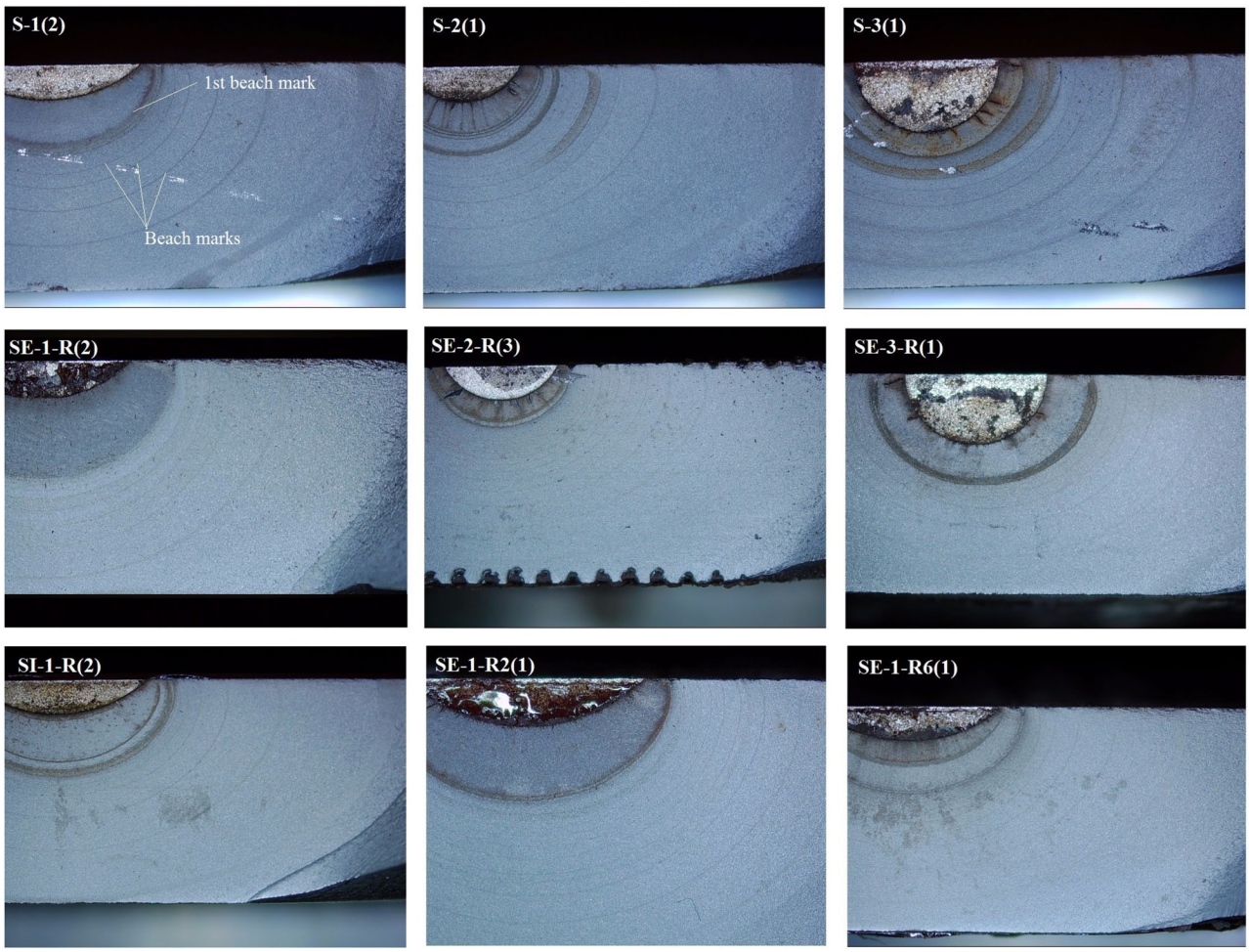

Figure 10. Beach marks on the cross-section of the steel plate specimens.

the asymmetric reinforcing geometry [32], as indicated in Figure 12. Eventually it let the stress value – combined the tensile stress and bending stress on the un-reinforced surface – become higher than the un-reinforced steel plates, resulting in a larger Stress Intensity Factor (SIF) and a higher FCGR. Here, we conduct a theoretical analysis to further understand the mechanism of the FRP reinforcement on the surface cracked steel plate. The out-of-plane bending on the FRP reinforced steel plate can be calculated as

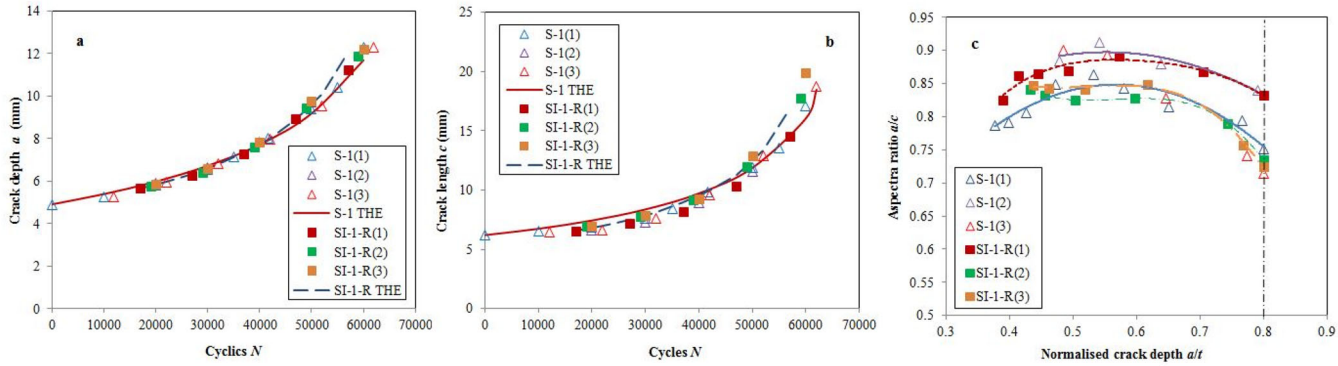

Figure 11. The experimental results of S-1 and SI-1-R: a) crack growth along depth direction; b) crack growth along length direction; c) *a*/*c* versus *a*/*t* ratio.

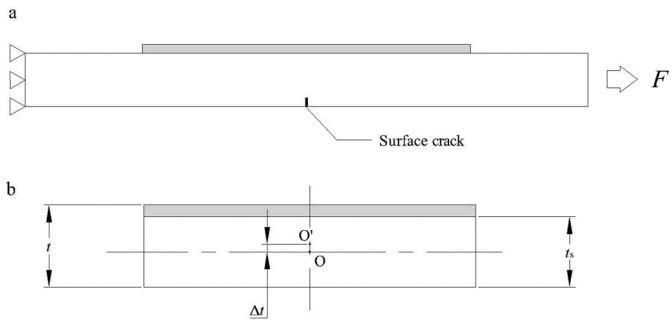

Figure 12. Gradient stress distribution in FRP reinforced steel plate caused by out-of-plane bending: a) FRP reinforced steel plates under pure tension; b) parameters of the FRP reinforcement system.

$$M = \frac{F}{t_s} \cdot \left[\int_{\frac{\Delta t}{2}}^{\frac{t_s}{2}+\frac{\Delta t}{2}} t dt - \int_{-\frac{\Delta t}{2}}^{\frac{t_s}{2}-\frac{\Delta t}{2}} t dt \right], \tag{1}$$

where t_s is the thickness of the steel plate, Δt is the distance between the centroid of the steel plate (O) and the centroid of the FRP reinforced steel plate (O') (see in Figure 12(b)), which is

$$\Delta t = (t - t_s)/2, \tag{2}$$

and t is the thickness of the FRP-reinforced steel plate (see in Figure 12(b)), which is

$$t = t_s + t_c + t_g + t_a, \tag{3}$$

where t_c, t_g, t_a are the thickness of the CFRP, GFRP, and the adhesive layer respectively. Thus the bending normal stress σ_b at the middle of the reversed surface can be calculated as

$$\sigma_b = \frac{M}{W} = \frac{M}{b \cdot (t)^2/6}. \tag{4}$$

The tensile normal stress σ_t along the length direction in the steel plate owing to the FRP reinforcement [17], can be calculated as

$$\sigma_t = \frac{E_s \cdot t_s}{E_s \cdot t_s + E_c \cdot t_c + E_g \cdot t_g + E_a \cdot t_a} \cdot \sigma_0, \tag{5}$$

where σ_0 is the in-plane tensile stress without FRP reinforcement, E_s, E_c, E_g, E_a are the tensile modulus of the steel, CFRP, GFRP, and the adhesive layer along the length direction respectively. Hence, owing to the out-of-plane bending moment, the problem is regarded as the surface crack growth in a steel plate subjected to combined tension and bending loads, where the SIF can be calculated by the Newman-Raju's Eq. (4), which is

$$K_I = (\sigma_t + H \cdot \sigma_b) \cdot \sqrt{\pi \cdot \frac{a}{Q}} \cdot F, \tag{6}$$

where σ_t and σ_b represents tension stress and bending stress, respectively, H is a correction function for the bending nominal stress, Q is the boundary correction factor for the surface crack profile. F is the boundary correction factor. Thus combined with the Paris' law [33], which is

$$da/dN = C \cdot (\Delta K_{Ia})^m, \tag{7}$$

$$dc/dN = C \cdot (\Delta K_{Ic})^m, \tag{8}$$

the crack growth rate along the length direction and depth direction are estimated, respectively. In Eqs. (7) and (8), da/dN and dc/dN are the crack growth rate along the depth direction and along the length direction, respectively, ΔK_{Ia} and ΔK_{Ia} are the range of SIFs of the deepest point and the surface point, respectively, C and m are two material constants, where C is 3.98×10^{-13} (SIF unit in MPa/mm$^{1/2}$), and m is 2.88, respectively [34]. Afterwards, by assuming a small amount of cycles, the increments of the crack length and depth are calculated. Eventually, it is possible to trace the surface crack growth along the two directions. The theoretical results match well with the experimental results, as shown in Figure 11. Therefore, besides the well-recognized stress decreasing effect owing to the FRP reinforcement, the out-of-plane bending moment caused by the asymmetric reinforcing geometry is a significant and non-negligible factor.

The increasing of the surface crack growth rate is further explained by the variation of the *da*/*dN*-*a* curve in Figure 13(a) and *dc*/*dN*-*c* curve in Figure 13(b). The da/dN-*a* and dc/dN-*c* relations are determined from the *a*-*N* and *c*-*N* results. The method is first evaluating the differential coefficient of the *a*-*N* and *c*-*N* curves, and then calculating each values of the da and dc based on each corresponding *a* and *c*. The *da*/*dN* of SI-1-R first increased to a higher value than the non-reinforced specimens, but then decreased evidently due to the decreasing stress (see in Figure 13(b)). While the *dc*/*dN* of SI-1-R were always higher than the *dc*/*dN* of S-1 specimens, owing to the higher stress value on the cracked

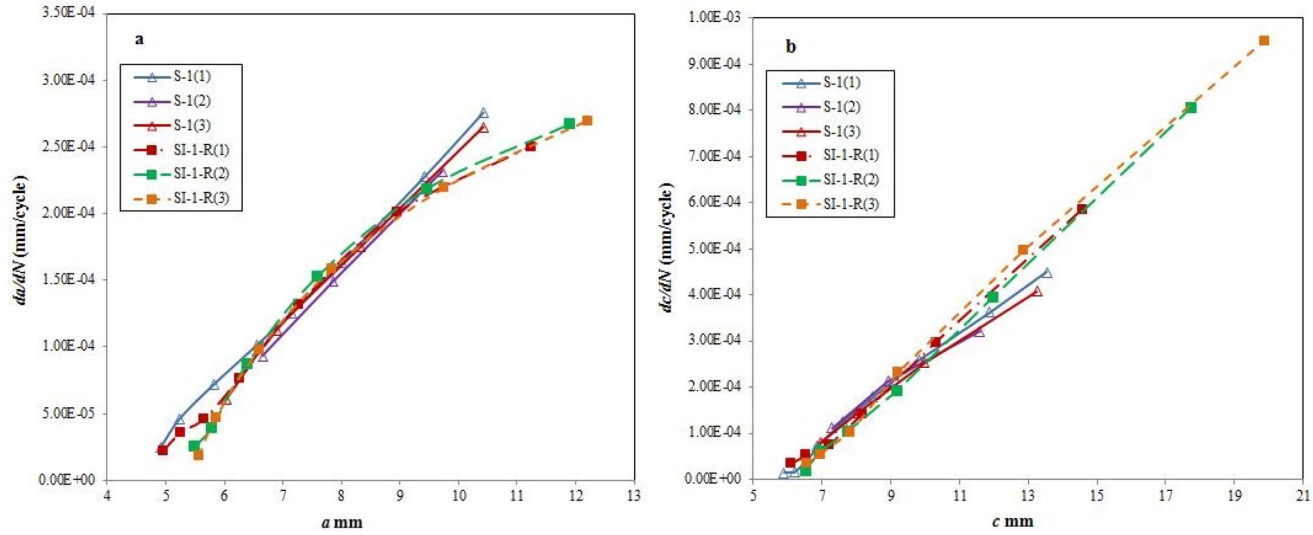

Figure 13. The FCGR of S-1 and SI-1-R of using four layers of CFRP: a) along the depth direction; b) along the length direction.

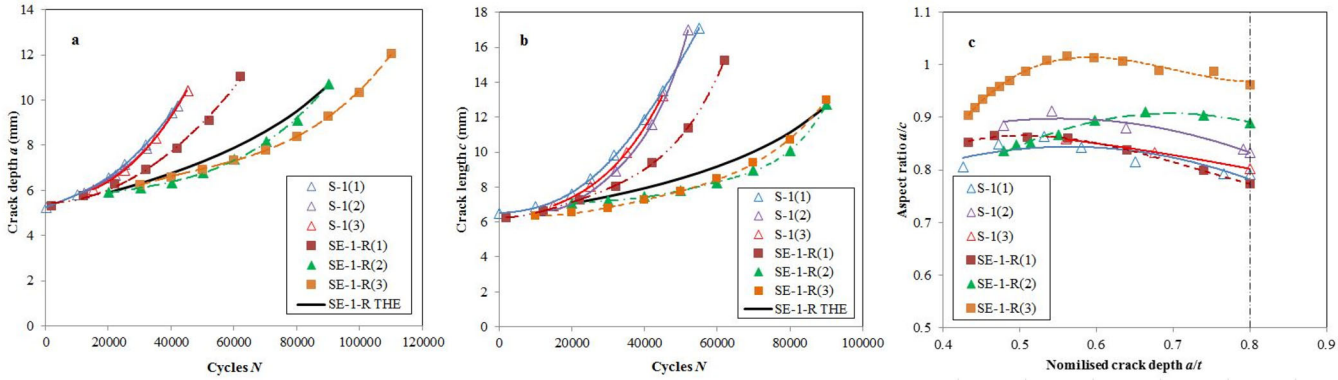

Figure 14. The experimental results of S-1 and SE-1-R of using four layers of CFRP: a) crack growth along depth direction; b) crack growth along length direction; c) *a*/*c* versus *a*/*t*.

surface caused by the out-of-plane bending moment. In addition, since there was no direct contact between the surface crack and the FRP reinforcement, the crack-bridging effect did not contribute to the decreasing of the SIF of the surface point; hence the FRP reinforcement did not evidently influence the preferred aspect ratios of the surface cracks, as shown in Figure 13(c).

5.2. FRP reinforcement on the cracked surface of the steel plates with different notch sizes

In this part, the results of FRP reinforcement on the cracked surface of specimens with three different crack sizes are analyzed. The results of *a*-*N* & *c*-*N* and d*a*/d*N*-*a* & d*c*/d*N*-*c* of the reinforced specimens are compared with the un-reinforced specimens. The abnormal crack growth behavior, i.e., the sudden growth of crack growth rate, is explained by the failure modes during the fatigue tests.

The surface crack growth results of the specimens in Group 5 by using the FRP patch to reinforce the cracked surface, i.e., SE-1-R, is shown in Figure 14. It demonstrated that there are two diverse results among the three reinforced specimens: the FRP reinforcement of SE-1-R(2) and SE-1-R(3) has significantly prolonged the residual fatigue life approximately around 130%, while only around 20% for SE-1-R(1) due to the early occurred edge debonding failure. The possible reason of the edge debonding failures is due to the overlarge stress concentration caused by the imperfect bond condition, i.e., surface treatment, non-uniform of adhesive thickness. Note that in this paper, the fatigue life is the cyclic index till the crack penetrating the wall thickness. In addition, when the crack penetrated the thickness, the specimens with effective reinforcement had shorter crack length. Finally, the preferred aspect ratio (*a*/*c* when *a*/*t* equals to 0.8) of the FRP reinforced with FRP is larger than the preferred aspect ratio of the un-reinforced specimens (in between 0.7 to 0.8), as shown in Figure 14(c). The preferred aspect ratio of SE-1-R(3), which no failure occurred, is around 1.0 owing to the FRP reinforcement; while the aspect ratio of SE-1-R(2) is larger than the unreinforced specimens but much smaller than the SE-1-R(3) due to the edge debonding and crack-induced debonding occurred the later stage. Since SE-1-R(1) has encountered serious edge debonding and crack-induced debonding at the beginning, its preferred aspect ratio is identical with the unreinforced specimens.

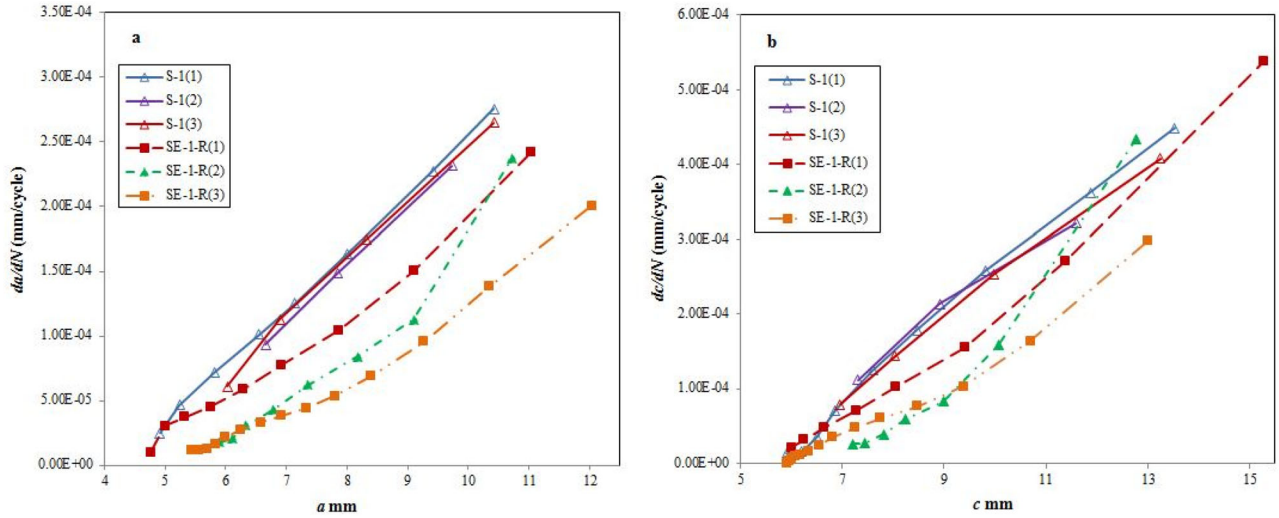

Figure 15. The FCGR of S-1 and SE-1-R of using four layers of CFRP: a) along the depth direction; b) along the length direction.

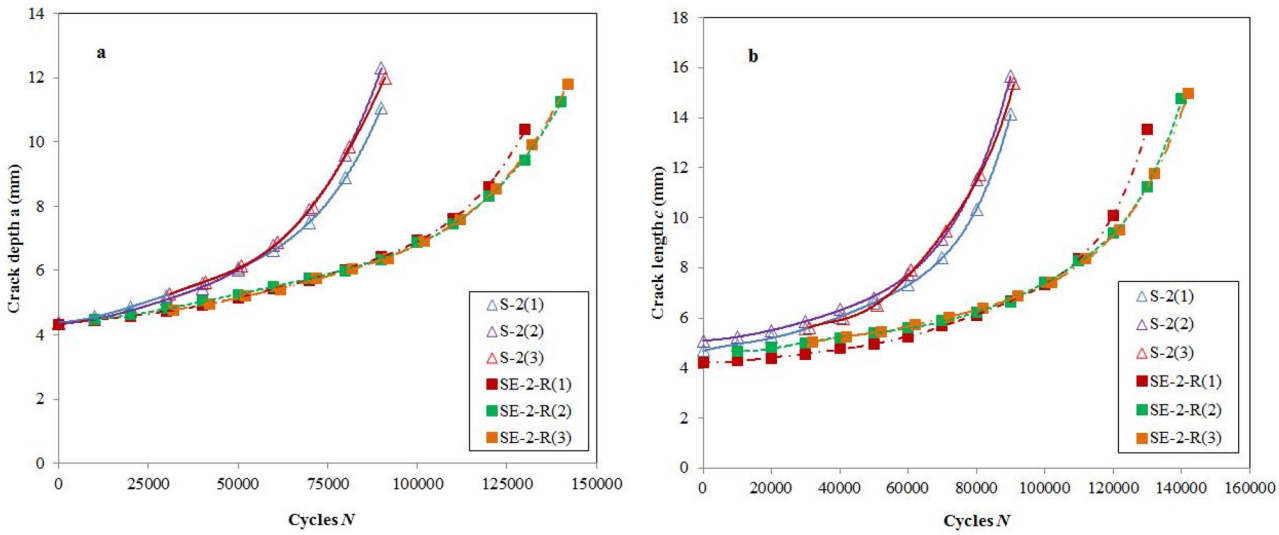

Figure 16. The experimental results of S-2 and SE-2-R: a) crack growth along depth direction; b) crack growth along length direction.

Since the crack surface crack in this case contacts with the FRP reinforcement – the surface crack locates on the compressed surface owing to the out-of-plane bending moment (despite the tensile stress), thus when evaluating the SIF of the surface crack, Eq. (6) can be modified as

$$K_{\mathrm{I}} = (\sigma_{\mathrm{t}} - H \cdot \sigma_{\mathrm{b}}) \cdot \sqrt{\pi \cdot \frac{a}{Q}} \cdot F. \tag{9}$$

Then through Eq. (9) and the Paris' law, the surface crack growth process along the depth and length direction can be evaluated. Figure 14 shows the good agreement between the theoretical results and the experimental results. While the theoretical analysis offers a slight non-conservative prediction of the surface crack growth rate, owing to the fact that the crack-bridging effect has not been taken into consideration.

Figure 15 illustrates that the FCGR of SE-1-R(1) is higher than the SE-1-R(2) and SE-1-R(3), due to the edge debonding failures occurring at the beginning of the fatigue tests (indicated in Table 5). Thus the less bonding area became not effective enough to decrease the SIF. Figure 15 also shows that an obvious rising trend of da/dN and dc/dN have been appeared on SE-1-R(2), induced by the edge debonding happened when a and c became larger than about 9.0 mm (in between 60,000 to 70,000 cycles). The edge debonding further triggered the crack-induced debonding, monitored by the strain gauges matrix (see in Figure 8 and in Table 5). Expect that, the FRP reinforcement of SE-1-R(3) had averagely decreased the FCGR along the depth direction of around 6.69×10^{-5} mm/cycle, while 1.25×10^{-4} mm/cycle along the length direction. Therefore, the FCGR along the length direction decreases more significantly than along the depth direction, which eventually resulting in the increasing the preferred aspect ratio.

The specimens of SE-2-R have the same initial notch depth ($a = 2.0$ mm) with the specimens of SE-1-R, but a shorter notch length. The results in Figure 16 illustrate that the results of SE-2-R repetitive specimens have good agreement with each other. Similar to SE-1-R(2), the FRP reinforcement has significantly prolonged the residual fatigue life. The specimen of SE-1-R(1) encountered a sudden increase at the later stage during the fatigue test,

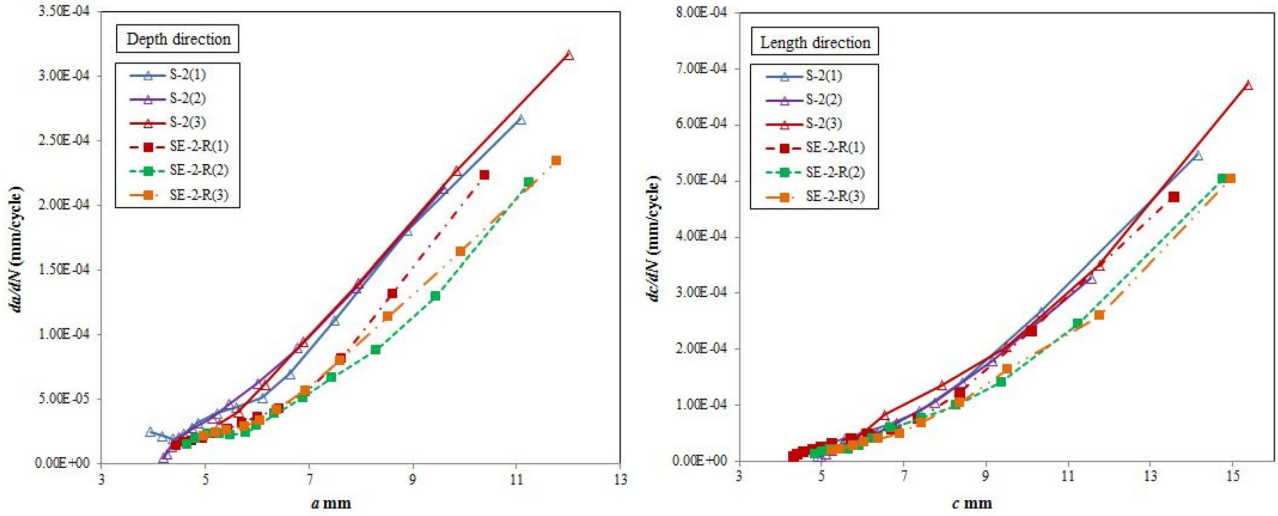

Figure 17. The FCGR of S-1 and SE-1-R of using four layers of CFRP: a) along the depth direction; b) along the length direction.

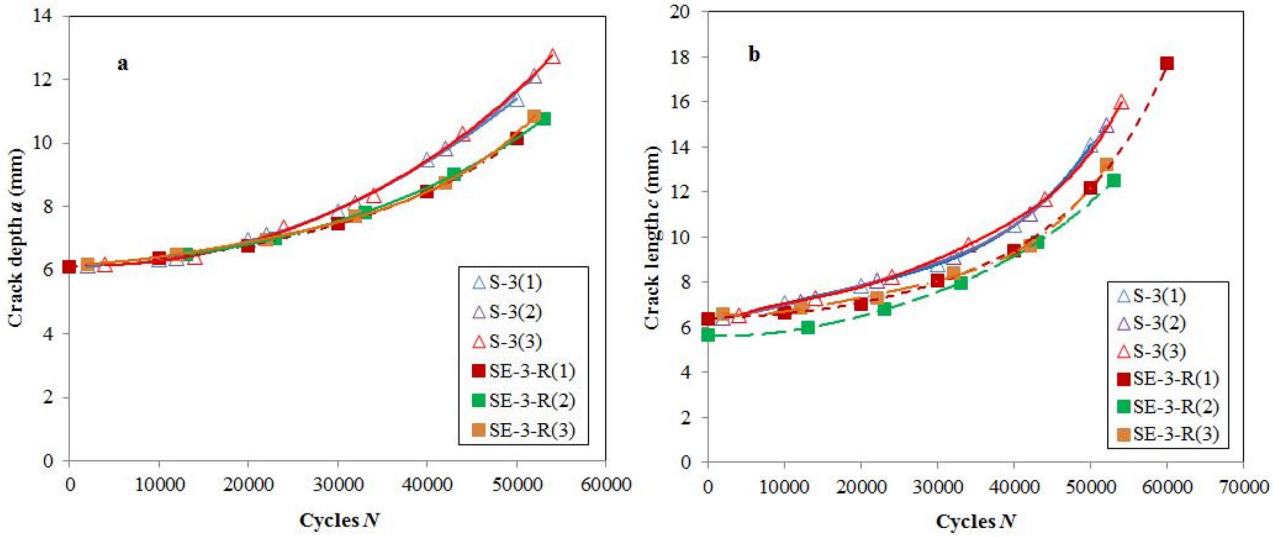

Figure 18. The experimental results of S-3 and SE-3-R: a) crack growth along depth direction; b) crack growth along length direction.

triggered by the edge debonding and crack-induced debonding. However, since the debonding failures occurred at the later stage, they did not cause considerable influence on the surface crack growth – specimen SE-2-R(1) had only around 3.5% less residual life than the other two reinforced specimens.

The *da*/*dN*-*a* and *dc*/*dN*-*c* curve in Figure 17 illustrates that the crack growth rates of SE-2-R(1) is higher than the SE-1-R(2) and SE-1-R(3) when *c* reached around 8.5 mm (in between 70,000 to 80,000 cycles), due to the occurrence of the edge debonding and the crack-induced debonding (indicated in Table 5). Except that, the FRP reinforcement has averagely decreased the FCGR (e.g., SE-2-R(2)) along the depth direction of 8.94×10^{-5} mm/cycle, 1.50×10^{-4} mm/cycle along the length direction.

However, using the FRP patch to reinforce large surface cracks was not as efficient as reinforcing smaller cracks. The reinforcement only had a minimal effect on reducing the FCGR of the specimens SE-3-R when the crack has already penetrated around half of the wall thickness, with only around 15%, as shown in Figure 18. The reason is not due to the absolute decreasing value of the FCGR, but the relative decreasing value. Thus the small relative decreasing FCGR eventually resulted in a limited extension of the fatigue life. Therefore, FRP reinforcement on surface cracked steel plates should be implemented as early as possible.

5.3. FRP reinforcement on the cracked surface of the steel plates using different number of CFRP layers

As is commonly acknowledged, applying more numbers of FRP laminates can promote the reduction the FCGR of the through-thickness cracks [35]. This has not yet been investigated on reinforcing the surface cracks. In this section, three different layers of CFRP, i.e. two layers, four layers, and six layers, are used in order to identify the influence of the number of CFRP layer on surface crack growth. Note that

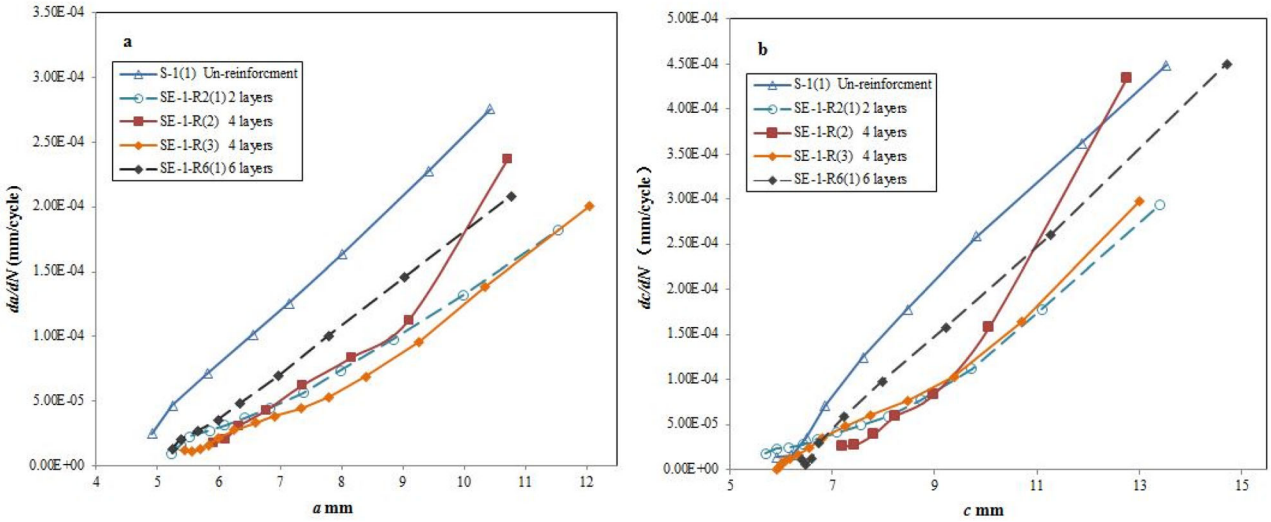

Figure 19. The FCGR of S-1 and SE-1-R of using different layers of CFRP: a) along the depth direction; b) along the length direction.

because of the limited number of specimens, only one specimen is prepared for the cases of using two layers and six layers.

The da/dN-a and dc/dN-c curves in Figure 19 show that FCGR of SE-1-R6(1) is higher than the other two FRP reinforced specimens shortly after the beginning of the test, due to the early occurred edge debonding failure. Despite the sudden FCGR increasing of specimen SE-1-R(2) when a and c reached about 9.0 mm, there is no big difference of the FCGR between the specimens using two layers of CFRP laminates and four layers of CFRP laminates. That indicates using more numbers of CFRP laminates of the single-side FRP patch might not be able to promote the effectiveness on reducing the FCGR of surface cracks.

6. Conclusions

Surface crack growth is a serious threat to the structure integrity of metallic structures. In this article, the surface crack growth in steel plates reinforced with the single-side FRP patch subjected to cyclic tension has been experimentally investigated. The effectiveness of FRP reinforcement on the surface crack growth has been analyzed. Besides, the possible failure modes as well as their effects on the surface crack growth are discussed. The conclusions can be drawn:

- In light of the single-side FRP reinforcement method, reinforcing the cracked surface has significantly prolonged the residual fatigue life, while reinforcing the reversed side resulted in the opposite consequence. The main reason is the out-of-plain bending moment induced by the asymmetric geometry. In this study, by using bond length of 150 mm and bond width of 60 mm and four layers of CFRP, the reinforcement has maximally prolonged the residual fatigue life of around 130%. In addition, the FCGR along the length direction decreased more significantly than along the depth direction, owing to the crack-bridging effect, resulting in a higher preferred aspect ratio.
- In this study, on account of using same bond length and width, there is negligible difference on the FCGR of applying two or four layers of CFRP laminates, which indicates that there might be an optimum number of bond layers. However, the analysis has been restricted by the limited number of specimens, further quantitative analysis will be presented along with other influential parameters in future studies, by means of numerical investigations.
- When using FRP to reinforce steel structures, the failures during the test which might influence the crack growth need attention, such as cohesion failures, FRP delamination, and interfacial debonding. In this study, during the fatigue test, the majority of the specimens (10 out of 14) did not encounter with any failures during the fatigue test – the FRP laminates were perfectly bonded on the steel substrate. The edge debonding occurred on two specimens at the beginning and two specimens at the later stage respectively. The early occurred edge debonding has largely weakened the effectiveness of FRP reinforcement, resulting in a minimal prolongation of the fatigue life of around 20%. The imperfect bond condition might be the culprit that has largely weakened the bond strength under the high load condition, which should be avoided by improving the surface treatment of the steel substrate.
- The concerned interfacial failure, i.e., crack-induced debonding, which is a serious threat of the FRP reinforcement system on repairing through-thickness cracks in steel plate, did not occur on the majority of the specimens. It means that when using FRP to reinforce surface cracked steel plates under cyclic tension, once the quality of the bond condition between the FRP laminate and steel substrate is guaranteed, the crack-induced debonding is not a threat to the FRP reinforcement on the surface cracked plate. In addition, even if the crack-induced debonding occurs, its negative influence on the FCGR was not serious, with only around 3.5% less residual life extension than the repetitive specimens on which no crack-induced debonding occurred.

Disclosure statement

No potential conflict of interest was reported by the authors.

Funding

The authors appreciate Department of Maritime and Transport Technology, Delft University of Technology, the Netherlands for sponsoring this research. The experimental investigation was supported by Overseas Expertise Introduction Project for Discipline Innovation – 111 project of Chinese Ministry of Education and State Administration of Foreign Experts Affair of P. R. China [grant number 444110356] and Department of Maritime and Transport Technology, Delft University of Technology, the Netherlands. The Key Laboratory of High Performance Ship Structure of the Chinese Ministry of Education is also appreciated for providing the experimental facilities. The first author would like to acknowledge the China Scholarship Council, P. R. China [grant number 201606950024] for funding his research.

ORCID

Zongchen Li http://orcid.org/0000-0003-4784-4684
Xiaoli Jiang http://orcid.org/0000-0001-5165-4942
Hans Hopman http://orcid.org/0000-0002-5404-5699

References

[1] J. Schijve, Fatigue of Structures and Materials. Springer Science & Business Media, The Netherlands, 2001.
[2] H. A. Richard and M. Sander, Fatigue Crack Growth. Springer, Berlin, 2016.
[3] Z. Li, X. Jiang, H. Hopman, L. Zhu, and Z. Liu, An investigation on the circumferential surface crack growth in steel pipes subjected to fatigue bending, Theor. Appl. Fract. Mech., vol. 105, pp. 102403, 2020.
[4] J. Newman, Jr and I. Raju, An empirical stress-intensity factor equation for the surface crack, Eng. Fract. Mech. , vol. 15, no. 1-2, pp. 185–192, 1981. DOI: 10.1016/0013-7944(81)90116-8.
[5] Z. Li, X. Jiang, Z. Liu, and, and H. Hopman, Internal surface crack growth in offshore rigid pipes reinforced with CFRP. In: ASME 2018 37th International Conference on Ocean, Offshore and Arctic Engineering. pp. V004T03A022-V004T03A022, 2018. DOI: 10.1115/OMAE2018-78060.
[6] Z. Li, X. Jiang, and H. Hopman, Numerical analysis on the SIF of internal surface cracks in steel pipes reinforced with CRS subjected to bending, Ships Offshore Struct., p. 1, 2019.
[7] L. Zhu, X. Tao, and L. Cengdian, Fatigue strength and crack propagation life of in-service high pressure tubular reactor under residual stress, Int. J. Press. Vessels Pip., vol. 75, no. 12, pp. 871–877, 1998. DOI: 10.1016/S0308-0161(98)00088-X.
[8] P. Singh, K. Vaze, V. Bhasin, H. Kushwaha, P. Gandhi, and D. R. Murthy, Crack initiation and growth behaviour of circumferentially cracked pipes under cyclic and monotonic loading, Int. J. Press. Vessels Pip, vol. 80, no. 9, pp. 629–640, 2003. DOI: 10.1016/S0308-0161(03)00132-7.
[9] Ž. Domazet, Comparison of fatigue crack retardation methods, Eng. Fail. Anal.., vol. 3, no. 2, pp. 137–147, 1996. DOI: 10.1016/1350-6307(96)00006-4.
[10] Z. Valadi, H. Bayesteh, and S. Mohammadi, XFEM fracture analysis of cracked pipeline with and without FRP composite repairs, Mech. Adv. Mater. Struct., vol. 23, pp. 1–12, 2018. DOI: 10.1080/15376494.2018.1529844.
[11] H. Yang, and X. Xu, Multi-sensor technology for B-spline modelling and deformation analysis of composite structures, Compos. Struct., vol. 224, pp. 111000, 2019. DOI: 10.1016/j.compstruct.2019.111000.
[12] X. Xu, R. Augello, and H. Yang, The generation and validation of a CUF-based FEA model with laser-based experiments, Mech. Adv. Mater. Struct., vol. 24, pp. 1–8, 2019.
[13] X. Xu, H. Yang, R. Augello, and E. Carrera, Optimized free-form surface modeling of point clouds from laser-based measurement, Mech. Adv. Mater. Struct., vol. 24, pp. 1–9, 2019.
[14] X. Zhao, and L. Zhang, State-of-the-art review on FRP strengthened steel structures, Eng. Struct, vol. 29, no. 8, pp. 1808–1823, 2007. DOI: 10.1016/j.engstruct.2006.10.006.
[15] Z. Li, X. Jiang, and G. Lodewijks, The latest development of reinforcement techniques on tubular joints, Progress in the Analysis and Design of Marine Structures, pp. 783–790, 2017. DOI: 10.1201/9781315157368-89.
[16] Z. Liu, K. Chen, Z. Li, and X. Jiang, Crack monitoring method for an FRP-strengthened steel structure based on an antenna sensor, Sensors, vol. 17, no. 10, pp. 2394, 2017. DOI: 10.3390/s17102394.
[17] Q. Yu, X. Zhao, Z. Xiao, T. Chen, and X. Gu, Evaluation of stress intensity factor for CFRP bonded steel plates, Adv. Struct. Eng., vol. 17, no. 12, pp. 1729–1746, 2014. DOI: 10.1260/1369-4332.17.12.1729.
[18] Q. Yu, T. Chen, X. Gu, X. Zhao, and Z. Xiao, Fatigue behaviour of CFRP strengthened steel plates with different degrees of damage, Thin Walled Struct., vol. 69, pp. 10–17, 2013. DOI: 10.1016/j.tws.2013.03.012.
[19] H. Wang, G. Wu, and Y. Pang, Theoretical and numerical study on stress intensity factors for FRP-strengthened steel plates with double-edged cracks, Sensors, vol. 18, no. 7, pp. 2356, 2018. DOI: 10.3390/s18072356.
[20] P. Colombi, G. Fava, and L. Sonzogni, Fatigue crack growth in CFRP-strengthened steel plates, Comp Part B: Eng., vol. 72, pp. 87–96, 2015. DOI: 10.1016/j.compositesb.2014.11.036.
[21] B. Zheng and M. Dawood, Debonding of carbon fiber–reinforced polymer patches from cracked steel elements under fatigue loading, J. Compos. Constr., vol. 20, no. 6, pp. 04016038, 2016. DOI: 10.1061/(ASCE)CC.1943-5614.0000694.
[22] H. Zarrinzadeh, M. Kabir, and A. Deylami, Crack growth and debonding analysis of an aluminum pipe repaired by composite patch under fatigue loading, Thin Wall Struct., vol. 112, pp. 140–148, 2017. DOI: 10.1016/j.tws.2016.12.023.
[23] B. Zheng and M. Dawood, Fatigue crack growth analysis of steel elements reinforced with shape memory alloy (SMA)/fiber reinforced polymer (FRP) composite patches, Compos. Struct., vol. 164, pp. 158–169, 2017. DOI: 10.1016/j.compstruct.2016.12.077.
[24] Z. Li, X. Jiang, and H. Hopman, Numerical investigation on surface crack growth in steel plates repaired with carbon fiber-reinforced polymer. In: ASME 2019 38th International Conference on Ocean, Offshore and Arctic Engineering, 2019. DOI: 10.1115/OMAE2019-95746.
[25] J. Chen and H. Pan, Stress intensity factor of semi-elliptical surface crack in a cylinder with hoop wrapped composite layer, Int. J. Press. Vessels Pip., vol. 110, pp. 77–81, 2013. DOI: 10.1016/j.ijpvp.2013.04.026.
[26] GJB, "Specification for 907A prefiled of military ship (in Chinese), GJB 6055-2007," ed: National military standard of P.R. China, 2007.
[27] GB, "Test method for properties of resin casting boby (in Chinese)," ed: National standard of P. R. China, 2008.
[28] E. ASTM, "2899," *Standard Test Method for Measurement of Initiation Toughness in Surface Cracks Under Tension and Bending*, vol. 3, 2015.
[29] T. Meshii, T. Tanaka, and K. Lu, T-Stress solutions for a semi-elliptical axial surface crack in a cylinder subjected to mode-I non-uniform stress distributions, Eng. Fract. Mech., vol. 77, no. 13, pp. 2467–2478, 2010. DOI: 10.1016/j.engfracmech.2010.06.007.
[30] A.T. Diamantoudis and G. Labeas, Stress intensity factors of semi-elliptical surface cracks in pressure vessels by global-local

finite element methodology, Eng. Fract. Mech., vol. 72, no. 9, pp. 1299–1312, 2005. DOI: 10.1016/j.engfracmech.2004.10.004.
[31] ASTM, "ASTM E647. Standard Test Method for Measurement of Fatigue Crack Growth Rates," ed, 1994.
[32] S. Naboulsi and S. Mall, Characterization of fatigue crack growth in aluminium panels with a bonded composite patch, Compos. Struct., vol. 37, no. 3-4, pp. 321–334, 1997. DOI: 10.1016/S0263-8223(98)80003-2.
[33] P. Paris and F. Erdogan, A critical analysis of crack propagation laws, J Basic Eng., vol. 85, no. 4, pp. 528–533, 1963. DOI: 10.1115/1.3656900.
[34] B. S. I. BS, "Guide on methods for assessing the acceptability of flaws in metallic structures," British Standard Institution, 2015.
[35] P. Colombi, A. Bassetti, and A. Nussbaumer, Analysis of cracked steel members reinforced by pre-stress composite patch, Fat. Frac. Eng. Mat. Struct., vol. 26, no. 1, pp. 59–66, 2003. DOI: 10.1046/j.1460-2695.2003.00598.x.

Appendix A. Fatigue test results of the surface crack growth

Table A1. Surface crack size along the depth and the length direction corresponding to cycle-index (units of *a* and *c* are in mm).

Specimen	S-1(1)		S-1(2)		S-1(3)		S-2(1)		S-2(2)		S-2(3)		S-3(1)		S-3(2)	
Cycles	*a*	*c*	*a*	*c*	*a*	*c*	*a*	*c*	*a*	*c*	*a*	*c*	*a*	*c*	*a*	*c*
0	4.64	5.90	5.89	6.66	6.03	6.95	4.17	4.52	4.18	4.90	5.27	5.63	5.40	5.78	6.15	6.42
10,000	4.91	6.20	6.66	7.30	6.89	8.03	4.38	4.7	4.25	4.99	5.63	5.98	5.55	6.08	6.38	7.16
20,000	5.24	6.50	7.85	8.92	8.32	9.98	4.59	4.92	4.35	5.10	6.15	6.54	5.92	6.48	7.13	8.06
30,000	5.82	6.86	9.73	11.59	10.42	13.25	4.85	5.26	4.49	5.26	6.89	7.92	6.35	7.06	8.14	9.13
40,000	6.55	7.59	$> t$	16.99	/	/	5.22	5.56	4.75	5.50	7.95	9.48	6.98	7.85	9.83	11.02
50,000	7.74	9.47	/	/	/	/	5.6	6.04	5.13	5.88	9.84	11.75	7.85	8.78	12.13	14.78
60,000	9.42	12.07	/	/	/	/	6.09	6.6	5.45	6.35	12.00	15.36	9.48	10.52	/	/
70,000	11.96	15.43	/	/	/	/	6.63	7.36	6.00	6.83	/	/	11.40	14.11	/	/
80,000	/	/	/	/	/	/	7.49	8.41	6.78	7.75	/	/	/	/	/	/
90,000	/	/	/	/	/	/	8.89	10.33	7.90	9.15	/	/	/	/	/	/
100,000	/	/	/	/	/	/	11.07	14.14	9.59	11.54	/	/	/	/	/	/
110,000	/	/	/	/	/	/	$> t$	17.97	12.30	15.66	/	/	/	/	/	/

Specimen	S-3(3)		SI-1-R(1)		SI-1-R(2)		SI-1-R(3)		SE-1-R(1)		SE-1-R(2)		SE-1-R(3)	
Cycles	*a*	*c*	*a*	*c*	*a*	*c*	*a*	*c*	*a*	*c*	*a*	*c*	*a*	*c*
0	5.86	5.78	4.95	6.00	5.49	6.53	5.56	6.56	4.77	5.87	5.78	/	6.25	6.33
10,000	5.93	6.08	5.26	6.10	5.78	6.94	5.86	6.95	5.00	6.00	5.90	7.06	6.59	6.54
20,000	6.18	6.52	5.66	6.54	6.39	7.75	6.59	7.83	5.33	6.25	6.10	7.20	6.91	6.80
30,000	6.42	7.32	6.26	7.20	7.59	9.17	7.84	9.23	5.75	6.64	6.33	7.44	7.34	7.25
40,000	7.35	8.23	7.28	8.16	9.45	11.97	9.75	12.88	6.28	7.28	6.77	7.81	7.80	7.75
50,000	8.37	9.66	8.95	10.31	11.90	17.75	12.2	19.88	6.92	8.04	7.36	8.23	8.39	8.48
60,000	10.32	11.69	11.24	14.57	/	/	/	/	7.87	9.40	8.17	8.98	9.27	9.39
70,000	12.70	16.02	/	/	/	/	/	/	9.10	11.39	9.10	10.07	10.34	10.70
80,000	/	/	/	/	/	/	/	/	11.03	15.27	10.72	12.76	12.04	13.00

Specimenen	SE-2-R(1)		SE-2-R(2)		SE-2-R(3)		SE-3-R(1)		SE-3-R(2)		SE-3-R(3)		SE-1-R2(1)		SE-1-R6(1)	
Cycles	*a*	*c*	*a*	*c*	*a*	*c*	*a*	*c*	*a*	*c*	*a*	*c*	*a*	*c*	*a*	*c*
0	4.04	4.01	3.96	4.33	4.78	5.05	5.40	5.78	5.82	5.36	6.21	6.60	5.23	5.7	5.24	6.41
10,000	4.09	4.05	4.02	4.36	4.97	5.26	5.55	6.08	6.12	5.66	6.52	6.88	5.38	5.91	5.38	6.48
20,000	4.15	4.10	4.10	4.43	5.21	5.46	5.92	6.48	6.51	5.97	6.98	7.32	5.51	6.15	5.66	6.59
30,000	4.22	4.16	4.22	4.54	5.42	5.76	6.35	7.06	7.01	6.81	7.69	8.40	5.85	6.42	5.98	6.74
40,000	4.32	4.23	4.48	4.68	5.76	6.04	6.98	7.85	7.83	7.97	8.75	9.63	6.09	6.71	6.35	7.22
50,000	4.44	4.31	4.64	4.83	6.05	6.38	7.85	8.78	9.01	9.78	10.86	13.23	6.42	7.09	6.96	7.97
60,000	4.58	4.40	4.82	5.01	6.38	6.89	9.48	10.52	10.77	12.54	$> t$	18.66	6.84	7.55	7.79	9.22
70,000	4.75	4.56	5.04	5.20	6.92	7.42	11.4	14.11	/	/	/	/	7.37	8.1	9.03	11.27
80,000	4.94	4.78	5.26	5.40	7.59	8.36	/	/	/	/	/	/	7.98	8.72	10.77	14.72
90,000	5.15	4.98	5.49	5.64	8.53	9.53	/	/	/	/	/	/	8.84	9.72	/	/
100,000	5.44	5.26	5.77	5.91	9.92	11.76	/	/	/	/	/	/	9.99	11.09	/	/
110,000	5.70	5.70	5.99	6.23	11.78	14.95	/	/	/	/	/	/	11.54	13.41	/	/
120,000	6.01	6.11	6.34	6.66	/	/	/	/	/	/	/	/	/	/	/	/
130,000	6.43	6.70	6.88	7.44	/	/	/	/	/	/	/	/	/	/	/	/
140,000	6.94	7.35	7.44	8.27	/	/	/	/	/	/	/	/	/	/	/	/
150,000	7.62	8.36	8.30	9.38	/	/	/	/	/	/	/	/	/	/	/	/
160,000	8.61	10.10	9.44	11.25	/	/	/	/	/	/	/	/	/	/	/	/
170,000	10.38	13.55	11.24	14.77	/	/	/	/	/	/	/	/	/	/	/	/